Sand ripples in liquids

Preprint submitted to ERCOFTAC Bulletin

Erick de Moraes Franklin

University of Campinas - UNICAMP, Campinas, Brazil

1 Introduction

A granular bed entrained as bed load may induce the formation of ripples and dunes [1]. Ripples are bedforms whose wavelengths scale with the grain diameter but not with the flow depth [2, 3] and are usually considered to be a result of initially two-dimensional bedforms that saturate eventually [4, 5]. On the contrary, dunes are bedforms whose wavelengths scale with both the flow field and the flow depth [2, 3] and may be considered as the result of coalescence of ripples [6, 7, 8, 9]. Ripples and dunes increase friction between the bed and fluid and are related to flooding, high pressure drops, and transients. The present article is a compilation of the referred papers [4], [5], [9], [10], [11].

2 Linear analysis

Many linear stability analyses have been conducted in the past decades on the stability of granular beds sheared by fluids. Although this approach has been criticized in the case of aquatic dunes [8, 9], it is justified in the case of aquatic ripples given the small aspect ratio of the initial bedforms from which ripples are formed.

Franklin [4] presented a linear stability analysis of a granular bed sheared by a turbulent liquid flow, without free-surface effects. The absence of a free surface is justified in the case of ripples, as these forms do not scale with the flow depth. Franklin's analysis was based on four equations, which describe the mass conservation of granular matter, fluid flow perturbation caused by the bed shape, the transport of granular matter by a fluid flow, and the relaxation effects related to the transport of grains. Although Franklin [4] presented the main mechanisms of ripple formation, he neglected the effects of the threshold shear stress for grain displacement, the bed compactness, and the settling velocity of grains on bed stability. These effects were considered by Franklin [11].

The conservation equations used in this analysis are the mass conservation of granular matter and the momentum balance between the liquid and the grains. The mass conservation of grains in two dimensions relates the local height of the bed, h, to the local transport rate (volumetric) of grains per unit width q:

$$\frac{\partial h}{\partial t} + \frac{1}{\phi}\frac{\partial q}{\partial x} = 0, \tag{1}$$

where t is the time, x is the longitudinal direction and ϕ is the bed compactness. The momentum balance between the liquid and the grains is usually obtained by dimensional analysis, as there is no consensus about the rheology of granular matter. Semi-empirical momentum balances between the liquid and the grains were proposed in the previous decades, and the obtained expressions relate the bed-load transport rate to the shear stress caused by fluid flow on a granular bed. The expression proposed by Meyer-Peter and Müller [12], one of the most frequently used transport rate equations, is based on data from exhaustive experiments, and for this reason, it is used in the present model. The volumetric transport rate of grains per unit width q_0 for a fully developed flow [12] is given by

$$q_0 = D_1 \left(\tau_0 - \tau_{th}\right)^{3/2}, \tag{2}$$

where τ_0 is the shear stress on the granular bed caused by the fully developed flow (the unperturbed, basic state flow described next) and τ_{th} is the threshold shear stress for the incipient motion of grains [1]. D_1 is given by:

$$D_1 = \frac{8}{\rho^{3/2}\left[\left(S-1\right)g\right]}, \tag{3}$$

where ρ is the specific mass of the liquid, $S = \rho_p/\rho$, ρ_p is the specific mass of the grain material and g is the acceleration of gravity. According to Eq. (3), D_1 is constant for given fluid and grain types.

The basic state corresponds to a fully-developed turbulent boundary layer over a flat granular bed. For a two-dimensional boundary layer, the fluid velocity profile is given by [13]

$$u = \frac{u_*}{\kappa}\ln\left(\frac{y}{y_0}\right), \tag{4}$$

where $u(y)$ is the longitudinal component of the mean velocity, $\kappa = 0.41$ is the von Kármán constant, y is the vertical distance from the bed, y_0 is the roughness length and $u_* = \rho^{-1/2}\tau_0^{1/2}$ is the shear velocity.

In the steady state regime without spatial variations (flat bed), the fully developed fluid flow is given by Eq. (4). In this case, the fluid flow and the flow rate of grains are in equilibrium. This means that the available momentum

for transporting grains as bed load is limited because part of the fluid momentum is transferred to the moving grains, which in turn transfer a part of the transferred fluid momentum to the fixed layers of the granular bed and another part to the interstitial fluid (mainly for liquids), until an equilibrium condition is reached. The equilibrium transport rate of grains is called *saturated transport rate* and is given by Eq. (2).

The origin of perturbations in this problem is the initial undulation of the granular bed. The bed undulation causes deviations from the basic state in both the fluid flow and the bed-load transport rate, thereby perturbing them. If the bed undulation is of a small aspect ratio, as expected for initial instabilities, the perturbations in the fluid flow and in the transport rate may be assumed as being small and a linear model can be used. The equations for these perturbations are presented next.

In the previous decades, many analytical works were focused on the perturbation of a turbulent boundary layer by bedforms. Among them, we cite Jackson and Hunt [14], Hunt et al. [15], and Weng et al. [16] here. Sauermann [17] and Kroy et al. [18, 19] simplified the results of Weng et al. [16] for surface stress and obtained an expression containing only the dominant physical effects of the perturbation. For a hill with local height h and a length $2L$ between the half-heights, they obtained the perturbation of the longitudinal shear stress (dimensionless):

$$\hat{\tau}_k = Ah(|k| + iBk), \tag{5}$$

where A and B are considered as constants, $k = 2\pi\lambda^{-1}$ is the longitudinal wavenumber, λ is the wavelength, and $i = \sqrt{-1}$. The shear stress on the bed surface is given as

$$\tau \;=\; \tau_0(1 + \hat{\tau}). \tag{6}$$

When the fluid flow is perturbed by the undulated bed, the bed-load transport rate varies locally. If equilibrium is assumed between the fluid flow and the bed-load transport rate, which is equivalent to neglecting the inertia of grains, then the transport rate is locally saturated and obtained by replacing τ_0 in Eq. (2) with τ (Eq. (6)). A convenient way to express this perturbed-saturated transport rate q_{sat} is:

$$\frac{q_{sat}}{q_0} \;=\; (1 + D_2\tau)^{3/2}\,, \tag{7}$$

where $D_2 \;=\; \tau_0\left(\tau_0 - \tau_{th}\right)^{-1}$ is a term that quantifies how far the flow is from the threshold. Fourrière et al. (2010) [8] proposed a more sophisticated expression for the perturbed-saturated transport rate, however, the form used here (Eq. (7)) is simpler while allowing to analyze threshold effects.

In the case of a spatially varying perturbed flow, a relaxation effect exists between the fluid and the grains owing to the inertia of the latter [20]. For this reason, the bed-load transport rate will lag behind the fluid flow by a certain distance, which is usually referred to as *saturation length*, L_{sat}. Andreotti et al. [20] proposed the following expression to take into account the relaxation effect:

$$\frac{\partial q}{\partial x} \;=\; \frac{q_{sat} - q}{L_{sat}}. \tag{8}$$

For the specific case of bed load under liquid flows, Charru (2006) [21] proposed that the saturation length L_{sat} is proportional to a deposition length $l_d = \frac{u_*}{U_s}d$:

$$L_{sat} \;=\; C_{sat}\frac{u_*}{U_s}d, \tag{9}$$

where U_s is the settling velocity of a single grain and C_{sat} is a constant of proportionality. The saturation length given by Eq. (9) is experimentally supported by Franklin and Charru (2011) [22].

Another parameter affecting bed stability is the local slope of the bed: the gravitational field weakens the transport of grains over positive slopes. One simple way to take into account this effect is to compute the effective shear stress perturbation by replacing B in Eq. (5) with $B_e = B - B_g/A$ so that the perturbed stress takes into consideration the grain weight and the shear between the grains, in addition to the shear caused by the fluid flow [21].

Taking into account that the initial instabilities are of a small aspect ratio, solutions h and q to Eq. (1), Eq. (6), Eq. (7), and Eq. (8) are plane waves. They can be decomposed into their normal modes as follows:

$$h(x,t) \;=\; He^{i(kx-\Omega t)} + c.c., \tag{10}$$

$$\frac{q(x,t)}{q_0} \;= 1 + Qe^{i(kx-\Omega t)} + c.c., \tag{11}$$

where $k \in \mathbb{R}$, $\lambda \in \mathbb{R}$, *c.c.* denotes "complex conjugate", and $H \in \mathbb{C}$ and $Q \in \mathbb{C}$ are the amplitudes. Let $\Omega \in \mathbb{C}$, $\Omega = \omega + i\sigma$, where $\omega \in \mathbb{R}$ is the angular frequency and $\sigma \in \mathbb{R}$ is the growth rate. Inserting the normal modes in Eq. (1), Eq. (6), Eq. (7), and Eq. (8), and finding the non-trivial solution gives the growth rate (Eq. (12)) and the phase velocity $c = \omega/k$ (Eq. (13)):

$$\sigma \;=\; \frac{3}{2}\frac{Aq_0D_2}{\phi}\frac{k^2\left(B_e - |k|L_{sat}\right)}{1 + \left(kL_{sat}\right)^2}, \tag{12}$$

$$c \;=\; \frac{3}{2}\frac{Aq_0D_2}{\phi}\frac{|k|\left(1 + B_eL_{sat}|k|\right)}{\left(1 + \left(kL_{sat}\right)^2\right)^2}. \tag{13}$$

2.1 Pressure-driven gas-liquid stratified flow

A common case in industry is the presence of bed load in stratified gas-liquid flows in horizontal ducts. Franklin [10] presented a model for the estimation of some bed-load characteristics. Based on parameters easily measurable in industry, the model can predict the local bed-load flow rates and the celerity and wavelength of instabilities appearing on the granular bed.

Following Cohen and Hanratty [23], Franklin [10] integrated in the y direction the x component of the momentum equation of both the mean gas and the mean liquid flows. For the gas, the integration was from $y = H_0$ to y, where $y = H_0$ is the liquid-gas interface at the basic state, and for the liquid the integration was from the granular bed surface at the basic state $y = h_0$ to $y = H_0$. As an output, Eq. (14) is obtained, relating the shear stress on the granular bed to the pressure gradient (dp/dx) of the flow and to the position of the maximum of the velocity profile at the basic state $y = a_0$.

$$\tau_0 \;=\; (a_0 + H_0)\left(-\frac{dp}{dx}\right) \tag{14}$$

The pressure gradient can be measured by pressure transducers installed along the flow-line. If they are absent, the pressure gradient may be estimated by the Lockhart-Martinelli correlations for gas-liquid flows [24, 25]. However, these correlations have limitations and intrinsic uncertainties are introduced. Franklin [10] performed a linear stability analysis and found that, for the most unstable mode within a long-wave approximation:

$$\lambda_{max} \;\sim\; \left(-\frac{dp}{dx}\right)^{(1/2)} \tag{15}$$

$$\sigma_{max} \;\sim\; \left(-\frac{dp}{dx}\right)^{(1/2)} \tag{16}$$

$$c_{G,max} \;\sim\; \left(-\frac{dp}{dx}\right) \tag{17}$$

2.2 Comparison with experimental results

Next, the results of the above-presented analysis are compared with published experimental results. In particular, the reported results of three experimental studies, which addressed the formation of aquatic ripples in closed conduits and pipes, are considered here. One of the studies was of Coleman et al. [26], who experimentally studied bed instabilities in a $6\,m$ long horizontal closed conduit with a rectangular cross section ($300\,mm$ wide by $100\,mm$ high) and employed water as the fluid medium and glass beads as the granular medium. The experiments were performed in a fully turbulent regime, with Reynolds numbers $Re = UH/\nu$ in the range $26000 < Re < 70000$ (where H is the channel height, ν is the kinematic viscosity, and U is the mean velocity of the fluid). Another study considered here is of Franklin [27], who experimentally studied initial instabilities in a $6\,m$ long horizontal closed conduit with a rectangular cross section ($120\,mm$ wide by $60\,mm$ high). The experiments were performed in a fully turbulent regime, with Reynolds numbers within the range $13000 < Re < 24000$. Finally, the study of Kuru et al. (1995) [28] is considered here. Kuru et al. (1995) [28] performed experiments on a $7m$ long, $31.1mm$ diameter horizontal pipe, and employed mixtures of water and glycerin as the fluid medium and glass beads as the granular medium.

Figure (1) shows a comparison of the curves of marginal stability obtained in this study [11] with the corresponding experimental data of Coleman et al. [26] and Franklin [27]. In this figure, the open diamonds and inverted triangles, taken from Coleman et al. [26], correspond to $d = 0.11\,mm$ and $d = 0.87\,mm$ glass spheres, respectively, under different shear velocities. The filled diamonds, circles, and squares, taken from Franklin [27], correspond to glass spheres with $d = 0.14\,mm$, $d = 0.25\,mm$, and $d = 0.53\,mm$, respectively, under different shear velocities.

Figure (1)(a) shows the curves of marginal stability in terms of u_* for different values of B_g, where the continuous, dashed, and dotted curves correspond to $B_g = 0$, $B_g = 0.01$, and $B_g = 0.02$, respectively. The model results are in agreement with experimental data, since all the measured ripples, with the exception of a few ripples with $d = 0.14mm$, lie in the predicted unstable regions. The measured ripples that are not in the unstable region are close to the marginal curves. This discrepancy may be related to experimental uncertainties, but a more probable reason pertains to some model parameters whose values are not well known. One of them is C_{sat}, whose value has not yet been measured in the aquatic case, and the other parameter is the threshold shear. In the present analysis, the Shields parameter at the bed-load threshold, i.e., $\theta_{th} = u_{*,th}/\left((S-1)gd\right)$, where $u_{*,th}$ is the corresponding shear velocity [1], was fixed at 0.04. However, there is no real consensus about this value, which may vary between 0.02 and 0.06 in the present case [29, 30, 31, 32].

Figure (1)(b) shows the curves of marginal stability in terms of d for different values of u_*, where all the parameters affected by d were varied accordingly. The dashed-dotted, continuous, dashed, and dotted curves correspond to $u_* = 0.01\,m/s$, $u_* = 0.02\,m/s$, $u_* = 0.04\,m/s$, and $u_* = 0.06\,m/s$, respectively. Considering that the open diamonds and inverted triangles correspond to $0.015\,m/s < u_* < 0.019\,m/s$ and $0.034\,m/s < u_* < 0.050\,m/s$, respectively, and that the filled diamonds, circles, and squares correspond to $0.011\,m/s < u_* < 0.020\,m/s$, $0.012\,m/s < u_* < 0.021\,m/s$, and $0.011\,m/s < u_* < 0.022\,m/s$, respectively, it can be confirmed that all the measured ripples lie in the predicted unstable regions and that the curves of marginal stability obtained in this study agree well with the published experimental data.

There is a lack of experiments in the scope of the formation of ripples in pressure-driven stratified liquid flows, even if there is a large number of industrial applications. However, the analysis can be compared with experimental data of pressure driven liquid flows carrying grains as bed load. Although the cases are different, the initial instabilities may

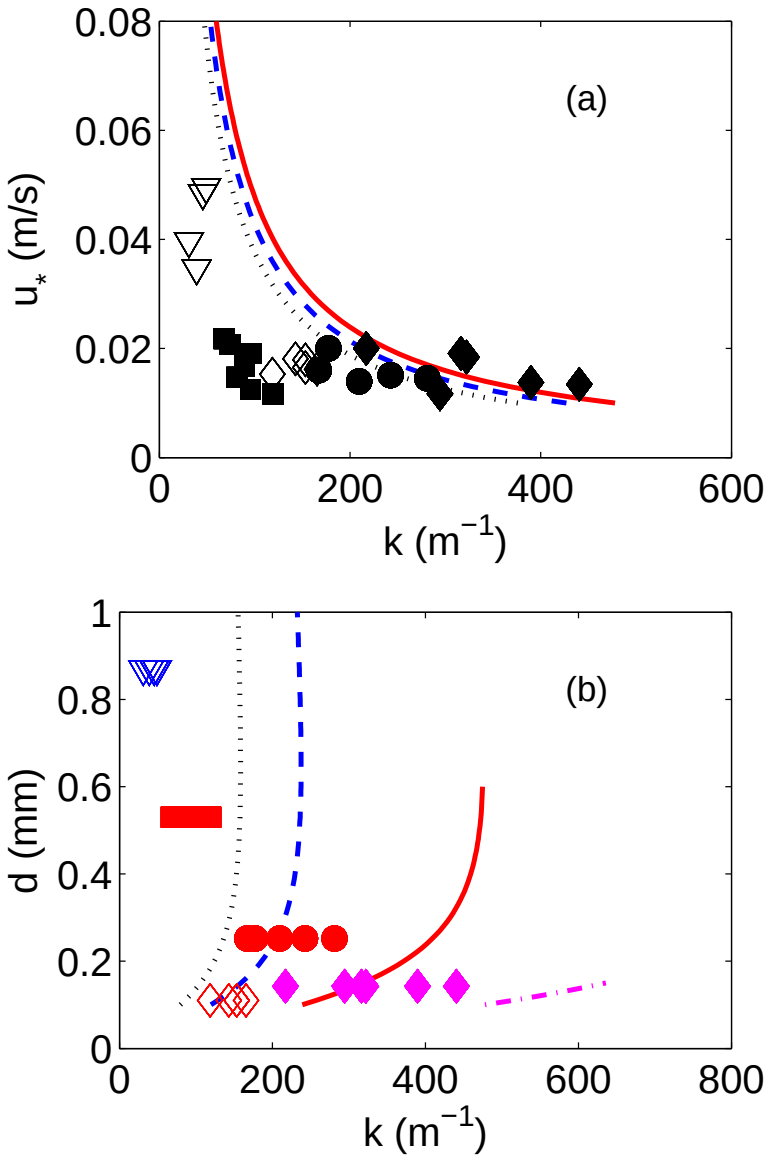

Figure 1: (a) Curves of marginal stability in terms of u_* for different values of B_g. The continuous, dashed and dotted curves correspond to $B_g = 0$, $B_g = 0.01$, and $B_g = 0.02$, respectively. (b) Curves of marginal stability in terms of d for different values of u_*, where all the parameters affected by d were also varied. The dashed-dotted, continuous, dashed, and dotted curves correspond to $u_* = 0.01\,m/s$, $u_* = 0.02\,m/s$, $u_* = 0.04\,m/s$, and $u_* = 0.06\,m/s$, respectively. The symbols correspond to experimental data and are described in the text. Figure extracted from Franklin (2015) [11]

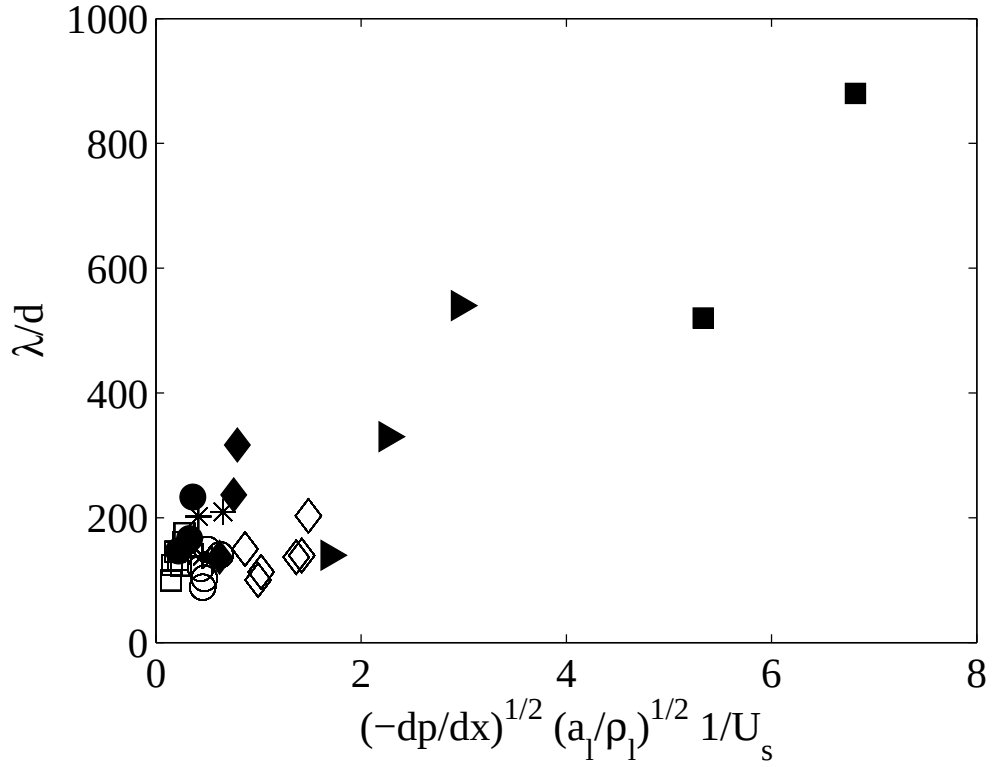

Figure 2: Dimensionless wavelength λ/d as a function of the square root of the dimensionless pressure gradient $(-dp/dx)^{1/2}(a_l/\rho_l)^{1/2}(1/U_s)$. Filled circles, lozenges, triangles and squares correspond to $d = 0.3mm$ and $\mu_l = 1cP$, $d = 0.3mm$ and $\mu_l = 2.2cP$, $d = 0.1mm$ and $\mu_l = 1cP$, and $d = 0.1mm$ and $\mu_l = 2.1cP$, respectively (experimental data of Kuru et al., 1995 [28]). Open lozenges, circles, squares and asterisks correspond to $d = 0.12mm$, $d = 0.20mm$ and $d = 0.50mm$ glass beads (in water), and to $d = 0.19mm$ zirconium beads (in water), respectively (experimental data of Franklin, 2008 [27]). Figure extracted from Franklin (2013) [10]

scale in a similar manner, given that the initial bedforms have small amplitudes and are not expected to be affected by the presence of a free surface. There studies of Kuru et al. (1995) [28] and Franklin (2008) [27] are considered here. In both works, the authors measured the wavelengths of the initial bedforms appearing on the granular bed.

The results of both works are summarized in Figure (2). In order to directly compare the experimental data with the present model (Eq. (15), Eq. (16) and Eq. (17)), Figure (2) presents the dimensionless wavelength λ/d of initial ripples as a function of the square root of the dimensionless pressure gradient $(-dp/dx)^{1/2}(a_l/\rho_l)^{1/2}(1/U_s)$, where a_l is the distance from the maximum of the liquid velocity profile to the bed. Filled symbols correspond to the experimental data of Kuru et al. (1995) [28] and open symbols to the experimental data of Franklin (2008) [27]. The description of each symbol is in the legend of Figure (2). The dimensionless parameters of Figure (2) come from Eq. (14) and Eq. (9), considering that $u_* = \sqrt{\tau_0/\rho_l}$ and changing $(a_0 + H_0)$ by a_l. In this case, we find that

$$\frac{\lambda}{d} \sim \left(-\frac{dp}{dx}\right)^{1/2} \left(\frac{a_l}{\rho_l}\right)^{1/2} \frac{1}{U_s} \tag{18}$$

If we take into account the relatively high uncertainties, often present in measurements of bed instabilities, the alignment of the experimental data in Figure (2) seems to support the results of the proposed model, that the wavelength of initial bedforms varies as $(-dp/dx)^{1/2}$, even if the experimental data were obtained for a case different from the scope of the model.

3 Weakly nonlinear analysis

In order to understand the evolution of ripples after the linear phase of the instability, i.e., in a time-scale greater than σ^{-1}, Franklin [5] presented a nonlinear stability analysis in the same scope of [4]. The approach used was the weakly nonlinear analysis [33], useful whenever a dominant mode exists. This means that the modes resonating with the dominant one will grow much faster than the others, which can be neglected. The analysis is then made on a bounded number of modes. A small modification in the analysis of [5] was proposed by Franklin [9]. Eq. (1) to Eq. (9) can be combined to give a single equation

$$\begin{aligned} &\partial_t h + B_1(h)^2 + B_2(\partial_x h)^2 \\ &+B_3 h\partial_x h + B_4 h + B_5\partial_x h - ch = 0 \end{aligned} \tag{19}$$

where c is the celerity of the bedforms and B_1 to B_5 involve q_0, L_{sat} and some constants, so that B_1 to B_5 are only functions of u_* and d. They may then be treated as constants in an analysis of a given granular bed submitted to a given fluid flow.

In the weakly nonlinear analysis we are interested in the early stages of the nonlinear instability, when the exponential growth is no longer valid and the nonlinear terms become pertinent. In this case, it is a reasonable assumption to consider that the celerity c of bedforms is approximately the celerity of the linear phase. The linear analysis showed that the celerity of the initial instabilities is given by $c \sim q_0/Lsat$, so that $c \sim u_*(u_* d/U_s)^{-1}$. With this assumption, c may be treated as a constant in an analysis of a given granular bed submitted to a given fluid flow. The last term of Eq. (19) is then considered here as varying with h.

In this problem, the large scales are limited by periodicity and the small ones by the discrete nature of the grains; therefore, a limited number of Fourier components can be considered. These modes can be inserted in Eq. (19) and the nonlinear terms maintained. Normalizing the problem by its characteristic length (k^{-1}), and inserting the normal modes into Eq. (19), one can find the following equation

$$\begin{aligned} &\tfrac{1}{2}\sum_{n=-\infty}^{\infty}\left[\frac{dA_n}{dt} + A_n(B_4 - c) + iB_5 n A_n\right] e^{inx} \\ &\quad +\tfrac{1}{2}\sum_{n=-\infty}^{\infty}\left[A_n^2 B_1 + B_2(inA_n)^2\right] e^{2inx} \\ &\quad +\tfrac{1}{2}\sum_{p=-\infty}^{\infty}\sum_{q=-\infty}^{\infty}\left[B_3 A_p iq A_q\right] e^{i(q+p)x} = 0 \end{aligned} \tag{20}$$

By inspecting Eq. (20), Franklin [5] proposed that the third term may resonate with the linear part if $q + p = n$. By keeping only the resonant terms of Eq. (20), we find

$$\frac{dA_n}{dt} \;=\; \sigma_n A_n \;+\; iB_3 \sum_{p=-\infty}^{\infty}\left[pA_{p+n}A_p^*\right] \tag{21}$$

where $\sigma_n \;=\; c - B_4 - inB_5$.

Inspecting Eq. (21), it can be seen that σ_n contains the linear part of the problem and that the nonlinearities are in the third term. If the latter is neglected, which can be done in the initial phase of the instability, we find that the solution is stable for $\sigma_n < 0$ and unstable for $\sigma_n > 0$. In this case, $c - B_4$ is the parameter controlling the threshold of the instability: given the scales of c, the basic state is stable when $u_*/L_{sat} < B_4$ and it is unstable when $u_*/L_{sat} > B_4$, and the constant B_4 may be seen as a threshold value. We retrieve the conclusion of the linear analysis of [4], that there is a cut-off wavelength that scales with both u_* and L_{sat}, the small wavelengths being stable.

Franklin [5] wrote Eq. (21) for the first three modes (for $n > 0$) and, on the onset of the instability, showed that: (i) the second and higher modes can be written as functions of the first mode; (ii) the first mode is a fundamental mode. An equation for the fundamental mode similar to the Landau Equation [33, 34] was then obtained

$$\frac{dA_1}{dt} \;=\; \sigma_1 A_1 \;-\; \kappa_L A_1 \left|A_1\right|^2 \;+\; O(A_1^5) \tag{22}$$

where $\kappa_L = -B_3^2/\sigma_2 > 0$.

From Eq. (22), we can see that the nonlinear term will saturate the instability in a time-scale greater than σ^{-1}: after the initial exponential growth, the instability will be attenuated and eventually reach a finite value for the amplitude, maintaining the same wavelength. This corresponds to a supercritical bifurcation. This result is corroborated by some experimental works [28, 27], as discussed in [5].

Acknowledgment

The author is grateful to FAPESP (grant no. 2012/19562-6), to CNPq (grant no. 471391/2013-1) and to FAEPEX/UNICAMP (conv. 519.292, project 0201/14) for the provided financial support.

References

[1] R. A. Bagnold, *The physics of blown sand and desert dunes*. Chapman and Hall, 1941.

[2] A. J. Raudkivi, *Loose boundary hydraulics*. Pergamon Press, 1 ed., 1976.

[3] F. Engelund and J. Fredsoe, "Sediment ripples and dunes," *Ann. Rev. Fluid Mech.*, vol. 14, pp. 13–37, 1982.

[4] E. M. Franklin, "Initial instabilities of a granular bed sheared by a turbulent liquid flow: length-scale determination," *J. Braz. Soc. Mech. Sci. Eng.*, vol. 32, no. 4, pp. 460–467, 2010.

[5] E. M. Franklin, "Nonlinear instabilities on a granular bed sheared by a turbulent liquid flow," *J. Braz. Soc. Mech. Sci. Eng.*, vol. 33, pp. 265–271, 2011.

[6] A. J. Raudkivi and H. H. Witte, "Development of bed features," *J. Hydraul. Eng.*, vol. 116, pp. 1063–1079, 1990.

[7] A. J. Raudkivi, "Transition from ripples to dunes," *J. Hydraul. Eng.*, vol. 132, pp. 1316–1320, 2006.

[8] A. Fourrière, P. Claudin, and B. Andreotti, "Bedforms in a turbulent stream: formation of ripples by primary linear instabilities and of dunes by nonlinear pattern coarsening," *J. Fluid Mech.*, vol. 649, pp. 287–328, 2010.

[9] E. M. Franklin, "Linear and nonlinear instabilities of a granular bed: determination of the scales of ripples and dunes in rivers," *Appl. Math. Model.*, vol. 36, pp. 1057–1067, 2012.

[10] E. M. Franklin, "Prediction of the bed-load transport by gas-liquid stratified flows in horizontal ducts," *Appl. Math. Model.*, vol. 37, pp. 5627–5636, 2013.

[11] E. M. Franklin, "Formation of sand ripples under a turbulent liquid flow," *Appl. Math. Model.*, 2015.

[12] E. Meyer-Peter and R. Müller, "Formulas for bed-load transport," in *Proc. 2nd Meeting of International Association for Hydraulic Research*, pp. 39–64, 1948.

[13] H. Schlichting, *Boundary-layer theory.* Springer, 2000.

[14] P. S. Jackson and J. C. R. Hunt, "Turbulent wind flow over a low hill," *Quart. J. R. Met. Soc.*, vol. 101, pp. 929–955, 1975.

[15] J. C. R. Hunt, S. Leibovich, and K. J. Richards, "Turbulent shear flows over low hills," *Quart. J. R. Met. Soc.*, vol. 114, pp. 1435–1470, 1988.

[16] W. S. Weng, J. C. R. Hunt, D. J. Carruthers, A. Warren, G. F. S. Wiggs, I. Livingstone, and I. Castro, "Air flow and sand transport over sand-dunes," *Acta Mechanica*, pp. 1–21, 1991.

[17] G. Sauermann, *Modeling of wind blown sand and desert dunes.* PhD thesis, Universität Stuttgart, 2001.

[18] K. Kroy, G. Sauermann, and H. J. Herrmann, "Minimal model for aeolian sand dunes," *Phys. Rev. E*, vol. 66, no. 031302, 2002.

[19] K. Kroy, G. Sauermann, and H. J. Herrmann, "Minimal model for sand dunes," *Phys. Rev. Lett.*, vol. 88, no. 054301, 2002.

[20] B. Andreotti, P. Claudin, and S. Douady, "Selection of dune shapes and velocities. part 2: A two-dimensional model," *Eur. Phys. J. B*, vol. 28, pp. 341–352, 2002.

[21] F. Charru, "Selection of the ripple length on a granular bed sheared by a liquid flow," *Phys. Fluids*, vol. 18, no. 121508, 2006.

[22] E. M. Franklin and F. Charru, "Subaqueous barchan dunes in turbulent shear flow. Part 1. Dune motion," *J. Fluid Mech.*, vol. 675, pp. 199–222, 2011.

[23] L. S. Cohen and T. J. Hanratty, "Effect of waves at a gas-liquid interface on a turbulent air flow," *J. Fluid Mech.*, vol. 31, pp. 467–479, 1968.

[24] R. C. Martinelli and D. B. Nelson, "Prediction of pressure drop during forced-circulation boiling of water," *Trans. ASME*, vol. 70, pp. 695–702, 1948.

[25] R. W. Lockhart and R. C. Martinelli, "Proposed correlation of data for isothermal two-phase, two-component flow in pipes," *Chem. Eng. Prog.*, vol. 45, pp. 39–48, 1949.

[26] S. E. Coleman, J. J. Fedele, and M. H. Garcia, "Closed-conduit bed-form initiation and development," *J. Hydraul. Eng.*, vol. 129(12), pp. 956–965, 2003.

[27] E. M. Franklin, *Dynamique de dunes isolées dans un écoulement cisaillé.* PhD thesis, Université de Toulouse, 2008.

[28] W. C. Kuru, D. T. Leighton, and M. J. McCready, "Formation of waves on a horizontal erodible bed of particles," *Int. J. Multiphase Flow*, vol. 21, no. 6, pp. 1123–1140, 1995.

[29] P. Mantz, "Incipient transport of fine grains and flakes by fluids - extended Shields diagram," *J. Hydraul. Div.*, vol. HY6, pp. 601–615, 1977.

[30] M. S. Yalin and E. Karahan, "Inception of sediment transport," *J. Hydraul. Div.*, vol. HY11, pp. 1433–1443, 1979.

[31] R. L. Soulsby and R. J. S. Whitehouse, "Threshold of sediment motion in coastal environments," in *13th Australasian Coastal and Engineering Conference and 6th Australasian Port and Harbour Conference*, (Christchurch, New Zealand), pp. 149–154, 1997.

[32] J. M. Buffington and D. R. Montgomery, "A systematic analysis of eight decades of incipient motion studies, with special reference to gravel-bedded rivers," *Water Resour. Res.*, vol. 33, pp. 1993–2029, 1997.

[33] L. D. Landau and E. M. Lifshitz, *Fluid mechanics.* Pergamon Press, 1959.

[34] P. G. Drazin and W. R. Reid, *Hydrodynamic Stability.* Cambridge University Press, 2 ed., 2004.